




Differential Rotation of the Chromosphere in the He I Absorption Line

K. J. Li^{1,2,3} , J. C. Xu¹, J. L. Xie^{1,3}, and W. Feng⁴

¹ Yunnan Observatories, CAS, Kunming 650011, People's Republic of China

² Center for Astronomical Mega-Science, Chinese Academy of Sciences, Beijing 100012, People's Republic of China

³ Key Laboratory of Solar Activity, National Astronomical Observatories, CAS, Beijing 100012, People's Republic of China

⁴ Research Center of Analysis and Measurement, Kunming University of Science and Technology, Kunming 650093, People's Republic of China; fengwen69@sina.cn

Received 2020 August 4; revised 2020 November 11; accepted 2020 November 12; published 2020 December 11

Abstract

Differential rotation is the basis of the solar dynamo theory. Synoptic maps of He I intensity from Carrington rotations 2032–2135 are utilized to investigate the differential rotation of the solar chromosphere in the He I absorption line. The chromosphere is surprisingly found to rotate faster than the photosphere below it. The anomalous heating of the chromosphere and corona has been a big problem in modern astronomy. It is speculated that the small-scale magnetic elements with magnetic flux in the range of $(2.9\text{--}32.0) \times 10^{18}$ Mx, which are anchored in the leptocline, heat the quiet chromosphere to present the anomalous temperature increase, causing it to rotate at the same rate as the leptocline. The differential of rotation rate in the chromosphere is found to be strengthened by strong magnetic fields, but in stark contrast, at the photosphere strong magnetic fields repress the differential of rotation rate. A plausible explanation is given for these findings.

Unified Astronomy Thesaurus concepts: [Solar rotation \(1524\)](#); [Solar chromosphere \(1479\)](#); [Solar activity \(1475\)](#)

Supporting material: [animation](#)

1. Introduction

The Sun is magnetic, and solar activity and variation are both related to solar magnetic fields (Fang et al. 2008). Solar differential rotation is a classical research topic in solar physics due to its close relationship with solar magnetic fields (Babcock 1961), and measurements of differential rotation in the solar atmosphere and especially in the solar interior can provide some clues for solar dynamo theory. Two kinds of methods have been utilized to measure the differential rotation in the solar atmosphere. One is direct observation measurements, such as positioning and tracking of solar long-life structures (tracers) and Doppler spectrum observations, and the other is the periodicity analyses of long-term solar activity indexes modulated by solar rotation (Howard 1984; Javaraiah 2003; Chandra et al. 2010; Vats & Chandra 2011; Bhatt et al. 2017; Li et al. 2019; Xiang et al. 2020). Additionally, helioseismic measurements have recently been used to detect interior motions of the Sun, such as the inner zonal and meridional flows, and the flows are the foundation for understanding the differential rotation of the solar atmosphere (Howe 2009; Komm et al. 2009, 2018). Sunspots are the most classical tracer to measure the rotation rate of the solar atmosphere. Generally magnetic elements in quiet regions rotate faster than sunspots in active regions (Howard 1984, 1990; Xiang et al. 2014; Xu & Gao 2016), and they both rotate faster than the photospheric atmosphere (Stenflo 1989; Beck 2000; Lamb 2017; Imada & Fujiyama 2019; Li et al. 2019; Bertello et al. 2020). Recently Sudar et al. (2016) and Li et al. (2019) found that the corona anomalously rotates faster than the photosphere below it, although temperature and rotation rate should theoretically decrease (actually increase) from the bottom of the atmosphere, the photosphere to a higher layer of the solar atmosphere, because thermal energy and material of the solar atmosphere flow outward from the photosphere. Combined with the

abnormal heating of the upper solar atmosphere is abnormally the rapid rotation of the coronal atmosphere.

The chromosphere is daily observed in the He I 10830 Å line at National Solar Observatory (NSO)/Kitt Peak (Livingston et al. 1976). In this study, synoptical maps observed in the line at NSO are utilized to determine the rotation rate of the chromosphere.

2. Differential Rotation of the Solar Quiet Chromosphere

The solar chromosphere had been routinely surveyed in the He I 10830 Å line by the Vacuum Telescope at NSO/Kitt Peak from 2005 July to 2013 March (Livingston et al. 1976; Harvey & Livingston 1994), and correspondingly, synoptic maps of He I intensity (I_{He}) from Carrington rotations 2032 to 2135 were obtained. They can be downloaded from the NSO at <ftp://nispdata.nso.edu/kpvt/synoptic/>, and the website <https://solis.nso.edu/0/vsm/aboutmaps.html> introduced how to create a synoptic map from daily observations. Each synoptic map of He I intensity was measured at 360 equidistant longitudes from 1° to 360° and 180 latitudes (φ s), and these measurement latitudes have 180 equal steps in the sine of the latitudes ($\sin(\varphi)$) ranging from -1 (the solar south pole) to $+1$ (the north pole). Here Figure 1 shows all synoptic maps and an individual map, the synoptic map at Carrington rotation 2057 as an example. The unit of He I line intensity in these synoptic maps is arbitrary but constant.

The He I line is in absorption at the solar disk (Fleck et al. 1994; Harvey 1994; Brajsa et al. 1996). Observations of the quiet chromosphere disk are unique in the He I line, that is, structures with strong magnetic field, such as general network bright points, bright calcium, and hydrogen flocculi are dark in the line, displaying absorption features with relatively low intensities, instead of bright structures in the chromosphere generally observed by other chromosphere lines, such as H_α , Ca II, Mg II, and so on (Harvey & Sheeley 1977; Golub et al. 1989; Fleck et al. 1994; Brajsa et al. 1996). Therefore, the quiet

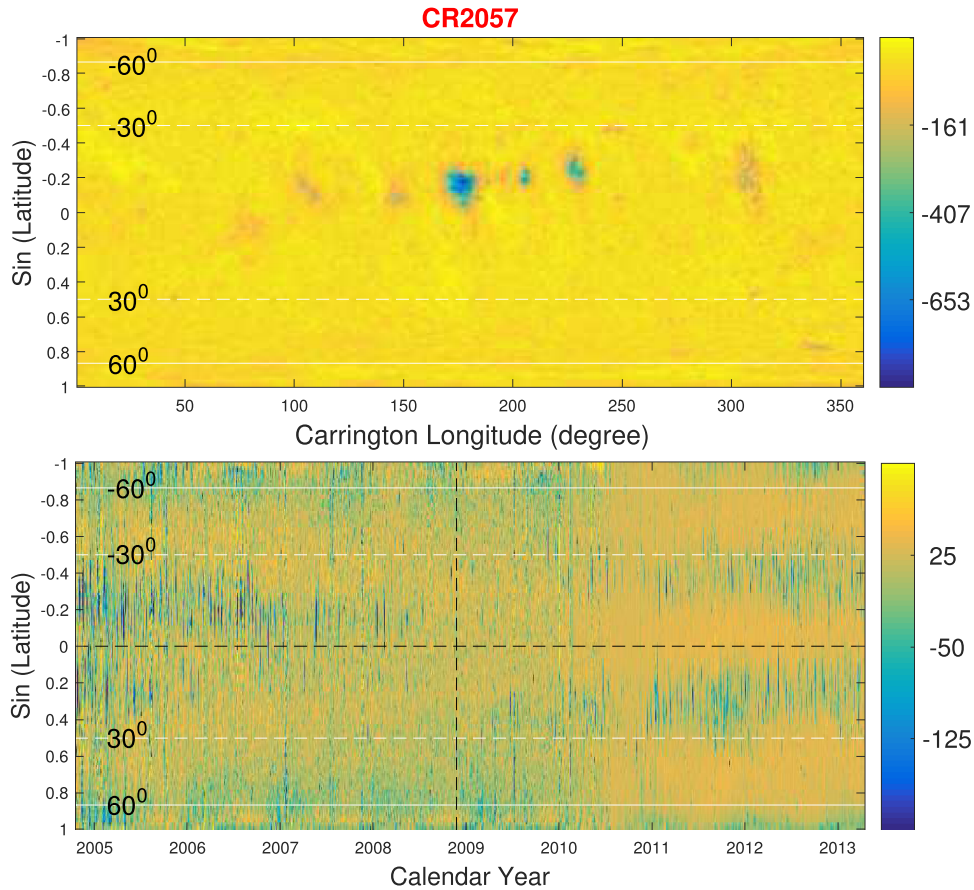


Figure 1. Top panel: the synoptic map of He I intensity at Carrington rotation 2057. Bottom panel: the time–latitude diagram of He I intensity in the interval of 2005 July to 2013 March. The white dashed (solid) lines show the latitudes of $\pm 30^\circ$ ($\pm 60^\circ$), and the vertical dashed line shows the minimum time of cycle 24.

chromosphere can be approximated through removing low-intensity values, and next in order to achieve this goal, we will count the intensity distribution of these synoptic maps to evaluate the proportion of low-intensity values in the entire data. Resultantly, Figure 2 shows the distribution of the original data points of I_{He} intensity in the range of $-200 \sim 100$, and those points beyond the range account only for 0.54% of the total points. We do not know why the range of I_{He} intensity is very wide, from the minimum of -2398.1 to the maximum of 3034.9 . When I_{He} is less than -50 , -30 , and -10 , the ratio of the number of data points to the total is 4.70%, 8.31%, and 17.35%, respectively. When I_{He} are in the range of $-200 \sim 100$, and meanwhile just those latitudes that are not larger than 30° are considered, the distribution of I_{He} is counted up, which is shown in the figure as well, and then when I_{He} is less than -50 , -30 , and -10 , the ratio of the number of data points to the total is 5.49%, 8.57%, and 17.84%, respectively. Therefore, active regions of sunspots with strong magnetic fields are basically excluded, if those I_{He} that are less than -10 are not considered, and then the quiet chromosphere can be approximated.

Because dark structures in the He I chromosphere are usually observed/measured in more than one day, we can derive their rotation rates. The classical autocorrelation analysis method for a time series is used to determine the rotation period of the series (Xu & Gao 2016; Li & Feng 2019). For a time series X_i ($i = 1, 2, \dots, N$), its autocorrelation coefficient is 1 when there is no relative shift, where N is the number of data points of the series. First, the series is one-point shifted with respect to itself,

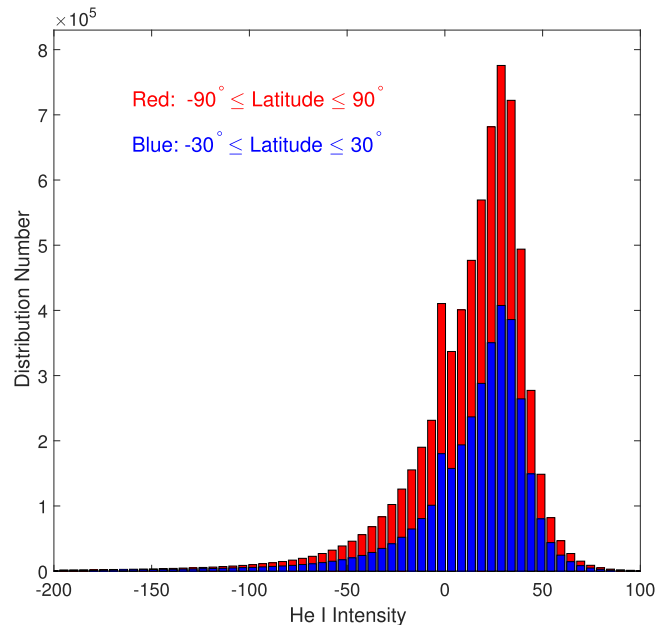


Figure 2. The distribution of He I intensity (I_{He}) in the range of $-200 \leq I_{\text{He}} \leq 100$ and meanwhile, respectively, at the full disk (the red histogram) and latitudes of -30° (the southern hemisphere) to 30° (the northern hemisphere).

and the unpaired endpoints of the two involved series are deleted. At this time, one series is X_i ($i = 1, 2, \dots, N-1$), the other is X_i ($i = 2, 3, \dots, N$), and the correlation coefficient (CC)

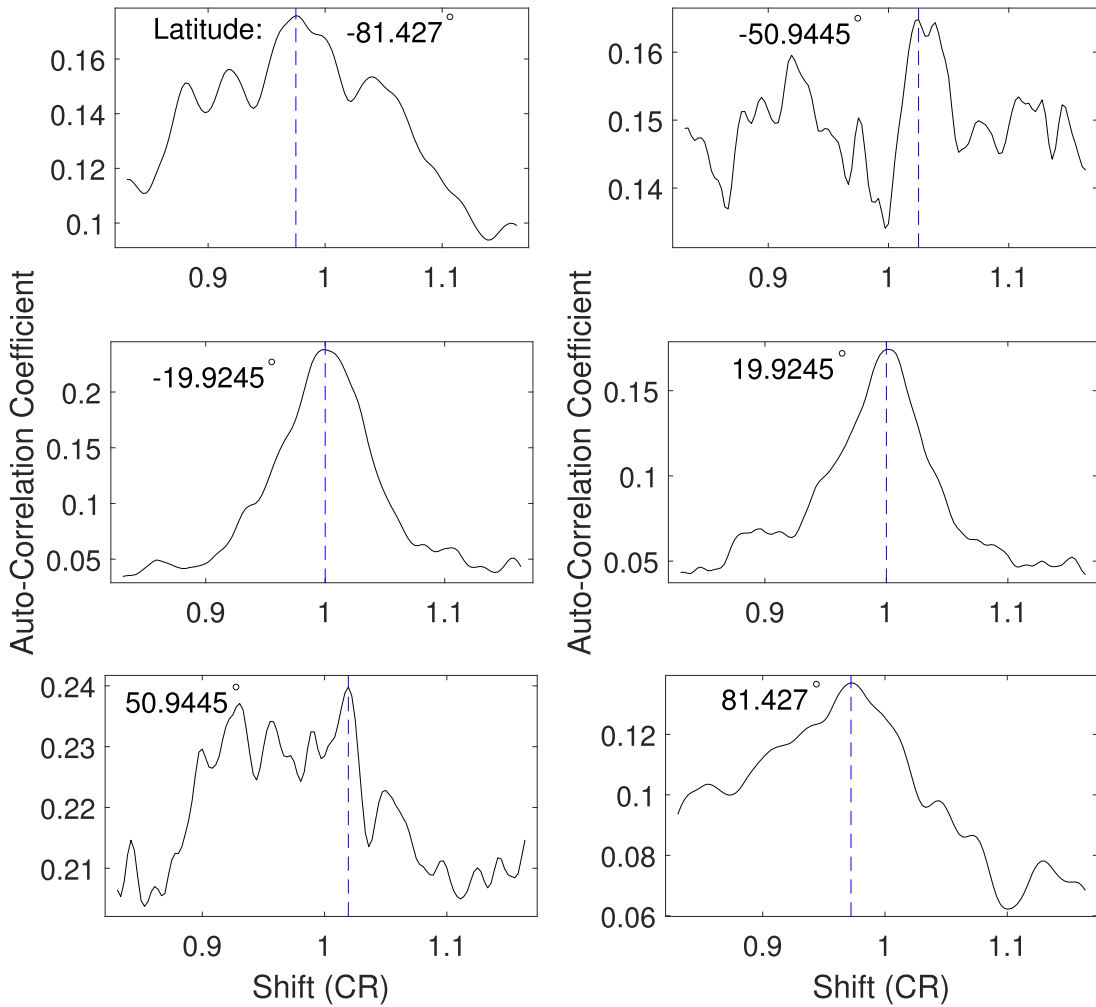


Figure 3. Autocorrelation coefficient (CC) of a time series of I_{He} at a certain latitude, varying with its relative phase shift. Six panels correspond to six time series of I_{He} whose latitudes are indicated at the top of each panel. The blue vertical dashed line in each panel shows the local maximum CC, whose abscissa shift is the synodic rotation period in CRs, and $1\text{CR} = 27.28$ days. An animation of this figure is available. The animation runs from -90° latitude to $+90^\circ$ latitude. The realtime duration is 54 s.

(An animation of this figure is available.)

can be obtained for these two series. Next, the original series is two-point shifted with respect to itself, and the unpaired endpoints of the two series are deleted. At this time, one series is X_i ($i = 1, 2, \dots, N-2$), the other is X_i ($i = 3, 4, \dots, N$), and a new correlation coefficient can be obtained then. The above process is repeated again and again, until relative phase shift is 500 data points. If there are no observations of I_{He} for an available Carrington rotation, I_{He} for the Carrington rotation are given to a very large negative value. When the negative value appears in the calculation of a correlation coefficient (CC), it and its paired value are ignored, and just the rest data are involved in the calculation. For a time series at a certain latitude, CC is calculated to vary with relative phase shift of the series versus itself, and the shift that corresponds to the local maximum CC around shifts of 27 days is regarded as the rotation period of the series. As an example Figure 3 shows the calculation results (CC varying with relative phase shift) of six time series. Finally, 180 rotation periods are obtained at the corresponding 180 measurement latitudes, whose calculation results are given in the animation of Figure 3. In Figure 3, CR is the length of a Carrington synodic rotation period, and $1\text{CR} = 27.275$ days; therefore, the resolution of relative phase

shifts is $27.275/360 \approx 0.076$ (days). After the synodic rotation period (P) of a series is obtained, its rotation rate can then be $P \times 13.199$ (in degrees/day; Shi & Xie 2013; Deng et al. 2020), which is shown in panel (I) of Figure 4, where 13.199 degrees/day is the rotation rate corresponding to the Carrington synodic period. Meanwhile, Panel (I) of Figure 5 shows CC corresponding to each obtained rotation period, and all CCs in the panel are significant at the 99% confidence level.

Differential rotation rate ($\Omega(\varphi)$) is generally expressed as

$$\Omega(\varphi) = A + B \sin^2(\varphi) + C \sin^4(\varphi).$$

The expression is used to fit those rotation rates whose latitudes are not higher respectively than 30° , 35° , and 40° . Resultantly, CCs for the fitting lines are 0.946, 0.963, and 0.938 in turn, which are all significant at the 99% confidence level.

Similarly, the autocorrelation analysis method is also used to determine rotation periods of those I_{He} that are not less, respectively, than -50 , -30 , and -10 , and as a result, panels (II), (III), and (IV) of Figure 4 show the obtained rotation rate at each measurement latitude in turn. Correspondingly, panels (II), (III), and (IV) of Figure 5 display CC at each measurement latitude in turn. For the sake of brevity, the rotation rates

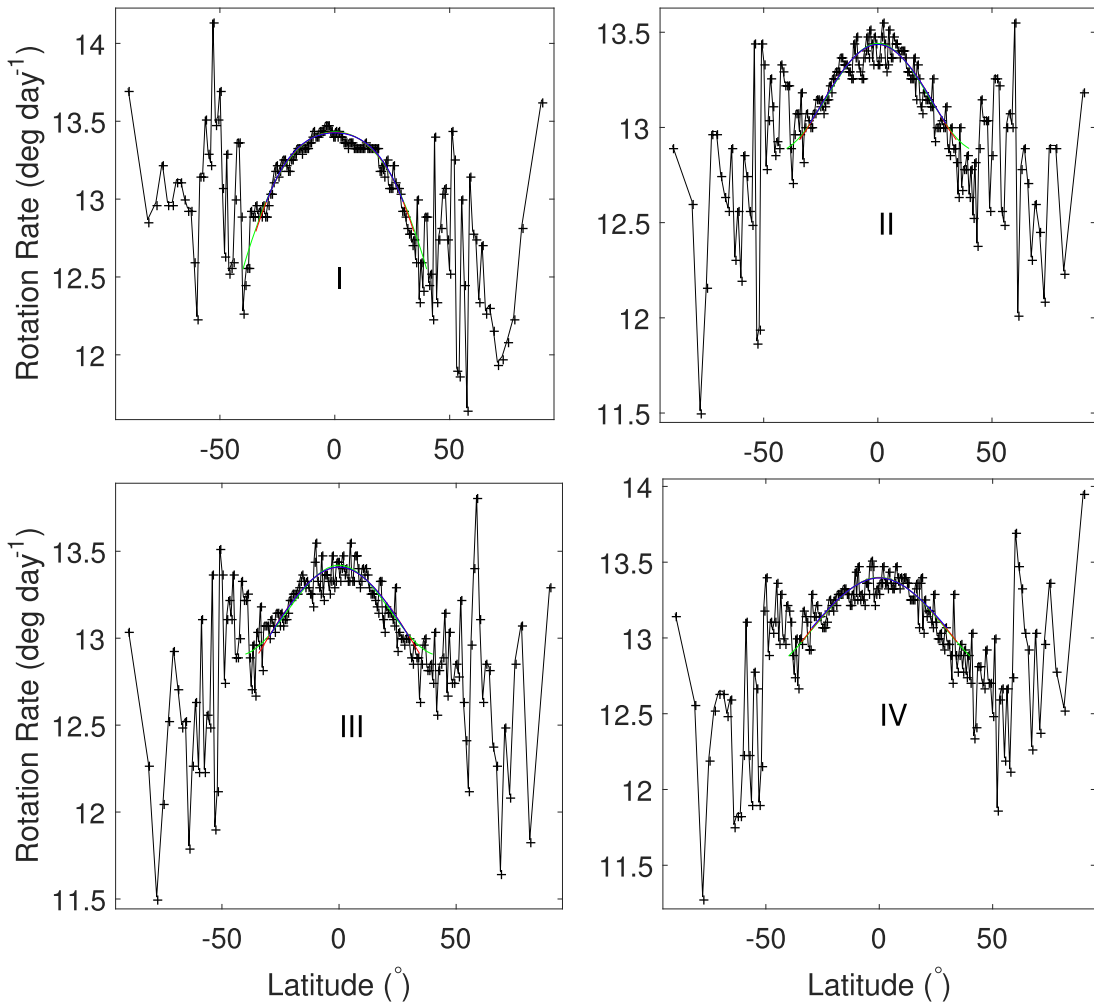


Figure 4. Panel (I): rotation rate (crosses in the black line) at each measurement latitude. The blue, red, and green lines are the fitting lines of those rotation rates whose latitudes are not greater than 30° , 35° , and 40° , respectively. Panel (II): the same as panel (I), but those I_{He} that are not less than -50 are considered. Panel (III): the same as panel (I), but those I_{He} that are not less than -30 are considered. Panel (IV): the same as panel (I), but those I_{He} that are not less than -10 are considered.

determined from I_{He} that are not less, respectively, than -50 , -30 , and -10 are called RR II, RR III, and RR IV in turn, and those determined from the complete original data are called RR I.

The expression is used to fit those rotation rates whose latitudes are not higher, respectively, than 30° , 35° , and 40° , and the obtained fitting lines are shown in Figure 4. These fitting lines are all highly significant. The fitting lines, respectively, for RR I to RR IV at latitudes that are not higher than 30° are put together in panel (I) of Figure 6. Figure 6 also shows the fitting lines, respectively, to RR I to RR IV at latitudes that are not higher than 35° in panel (II), and displayed in panel (III) are the fitting lines, respectively, to RR I to RR IV at latitudes that are not higher than 40° . As Figure 6 displays, rotation slightly becomes fast at low latitudes after eliminating the influence of strong magnetic fields of active regions, and this result is hardly affected by the low-latitude range considered. The Doppler rotation rate of the photosphere is also drawn in Figure 6, which was given by Snodgrass et al. (1984). The Doppler rotation rate is less than the rotation rate of the quiet chromosphere, and the (quiet) chromosphere rotates faster than the photosphere overall.

RR I whose latitudes are not higher, respectively, than 60° , 70° , and 80° are fitted with the following expression of rotation

rate, $\Omega(\varphi) = A + B \sin^2(\varphi) + C \sin^4(\varphi) + D \sin^6(\varphi)$, and as a result the obtained fitting lines are shown in panel (I) of Figure 7. These fitting lines are all highly significant. Due to low rotation rates around latitudes of about 50° , the fitting line to the latitudes that are not higher than 60° does not show a monotonous increase from low to high latitudes, but the other two fitting lines do.

Similarly, the expression is used to respectively fit RR II, RR III, and RR IV, at latitudes that are not higher, respectively, than 60° , 70° , and 80° , and as a result panels (II), (III), and (IV) of Figure 7 correspondingly display the fitting lines in turn. All of these fitting lines show a clear decreasing trend of rotation rate from low to high latitudes. Therefore, for the quiet chromosphere, rotation rate decreases from the equator to high latitudes of about $70^\circ \sim 80^\circ$ on the whole, and at latitudes of about 40° onward, the rotation rate fluctuates greatly.

3. Conclusions and Discussion

Synoptic maps of He I intensity, which are measured in the interval of 2005 July to 2013 March, are used to determine the rotation rate of the full-disk chromosphere observed in the He I 10830 Å absorption line. In the two cases of subtracting and not subtracting large magnetic-field values in active regions from the original data, the chromosphere is surprisingly found to

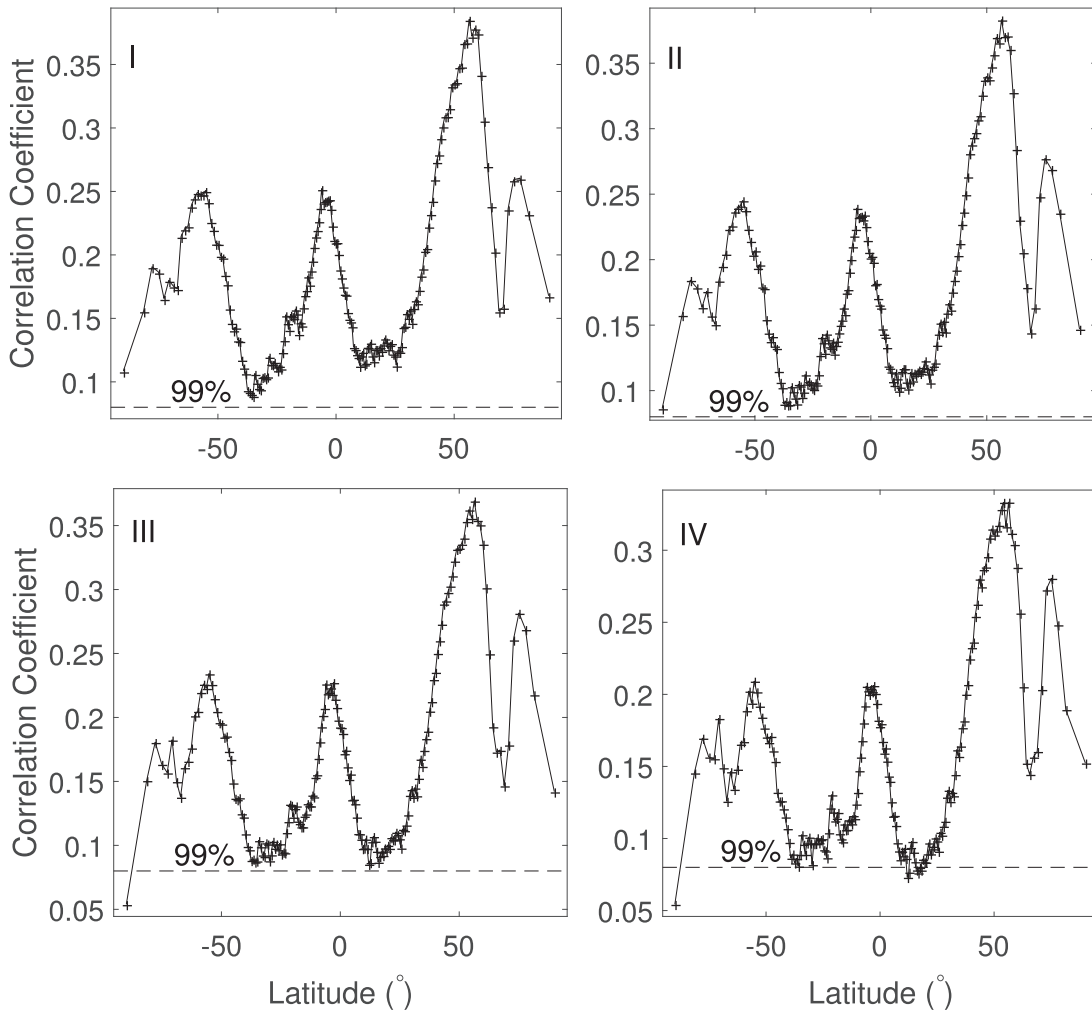


Figure 5. Panel (I): autocorrelation coefficient (crosses in the solid line) corresponding to the determined rotation period for a series of I_{He} at a measurement latitude. The dashed line shows the 99% confidence level. Panel (II): the same as panel (I), but those I_{He} that are not less than -50 are considered. Panel (III): the same as panel (I), but those I_{He} that are not less than -30 are considered. Panel (IV): the same as panel (I), but those I_{He} that are not less than -10 are considered.

rotate faster than the photosphere beneath it. Energy and material flow from the solar interior, through the photosphere to the chromosphere. Since the rotation of the chromosphere is obviously different from the photosphere rotation, the driving force for the chromosphere to rotate in this way is certainly from the solar interior, not from the photosphere.

Helioseismic measurements indicate that, at and just at the depths (the so-called leptocone) of $0.99 R_{\odot}$ to near $1 R_{\odot}$ of the solar interior, the long-term variation of the solar seismic radius is in antiphase with the Schwabe cycle, and the in situ magnetic fields are generated (Lefebvre et al. 2009); here R_{\odot} is the solar radius. The quiet chromosphere is found to be also in antiphase with the Schwabe cycle (Li & Feng 2020). Therefore, the driving force for the quiet chromosphere to rotate in such a way is believed to come from the leptocone in all probability, since the two present the same cycle phase. The small-scale magnetic elements (SMEs) whose magnetic flux spans $(2.9\text{--}32.0) \times 10^{18}$ Mx are in antiphase with the Schwabe cycle and distributed all over the solar disk (Jin et al. 2011; Jin & Wang 2012). They are thought to be the “in situ magnetic fields” generated in the leptocone, due to their same cycle phase. It is these small-scale magnetic elements that heat the chromosphere to lead to its formation, so that its rotation is traced by the rotation of the leptocone. Therefore, the quiet

chromosphere, SMEs, and the leptocone are all in antiphase with the solar cycle. Temperature changes from the outward decrease in the photosphere to the outward increase in the chromosphere. Studies of modern observations, theory, and statistics have showed that the quiet chromosphere is heated mainly by small-scale magnetic activities (Parker 1991; De Pontieu et al. 2017; Li et al. 2018), supporting the primary role of the magnetic elements in the heating and formation of the quiet chromosphere. The magnetic elements are anchored in the solar interior, connecting the chromosphere to the leptocone and transmitting the long-term evolution characteristics of the leptocone to the quiet chromosphere. Small-scale magnetic activities not only cause the quiet chromosphere to be abnormally heated, but also cause it to abnormally rotate faster than the photosphere plasma.

The rotation rate of small-scale magnetic elements is generally larger than that of sunspots, and they both are larger than that of plasma in the photosphere (Stenflo 1989; Howard 1996; Xiang et al. 2014; Xu & Gao 2016; Lamb 2017). This is the reason why the rotation rate of the quiet chromosphere is found here to be larger than that of the photosphere.

When strong magnetic fields are not eliminated, the rotation rate of the chromosphere decreases from the equator to middle

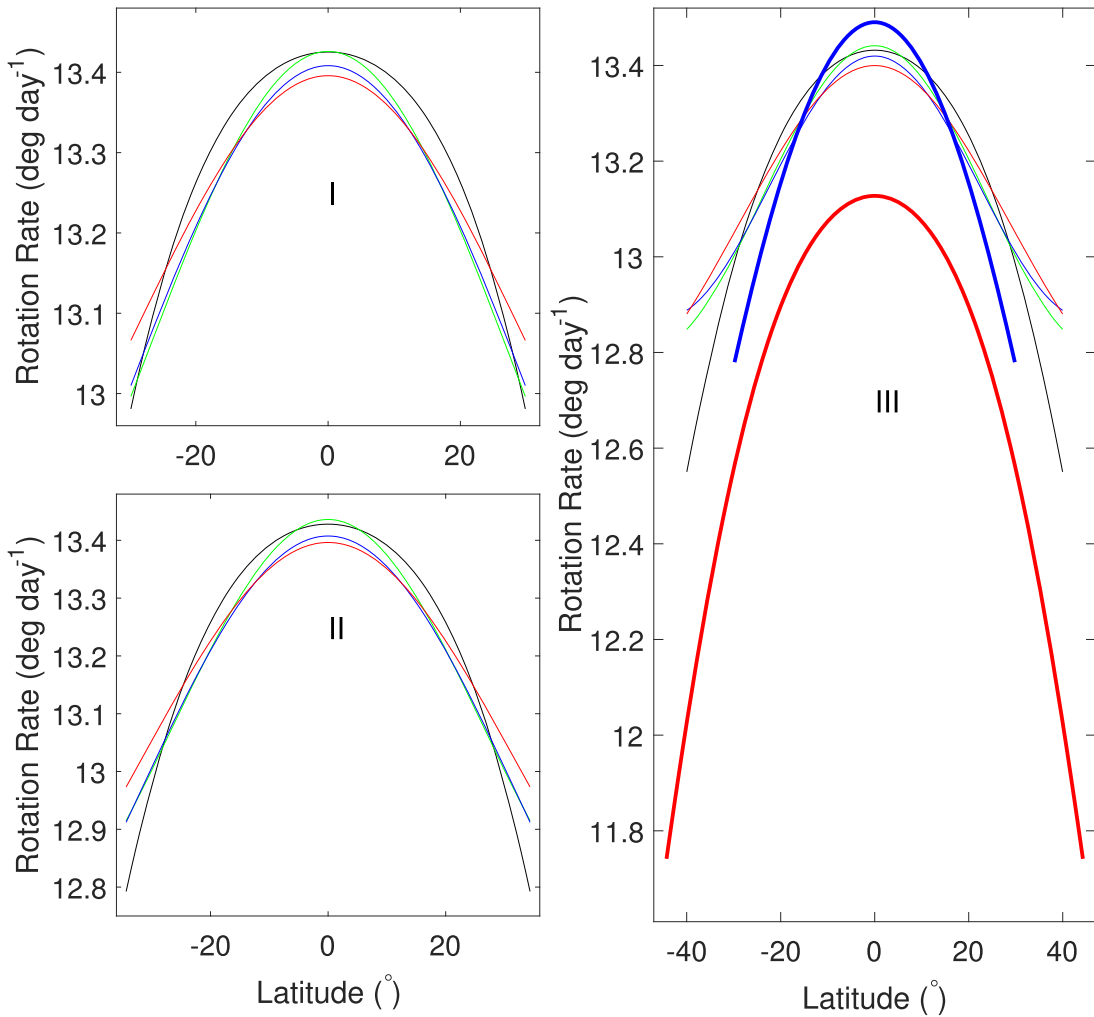


Figure 6. Panel (I): the fitting lines, respectively, to RR I (the black solid line), RR II (the green line), RR III (the blue thin line), and RR IV (the red thin line), at latitudes that are not greater than 30° . Panel (II): the same as panel (I), but at latitudes that are not greater than 35° , instead are of 30° . Panel (III): the same as panel (I), but at latitudes that are not greater than 40° , instead of 30° . In panel (III), the red thick line shows the rotation rate of the photosphere, which is determined in the spectrum method by Snodgrass et al. (1984), and the blue thick lines show the rotation rate of sunspots, which is given by Howard (1996).

latitudes faster than that when they are eliminated, and further, the more data points of strong magnetic fields are eliminated, the slower the rotation rate of the chromosphere decreases from the equator to middle latitudes. This means that strong magnetic fields should strengthen the differential of rotation rate. However, in sharp contrast, strong magnetic fields are found to repress the differential of rotation rate in the photosphere (Brajsa et al. 2006; Li et al. 2013). Sunspots generally appear at low latitudes ($8^\circ \sim 35^\circ$), and their rotation rates are shown in Figure 6, which come from Howard (1996). As the figure shows, the rotation rate of sunspots is lower than that of the quiet chromosphere at the low latitudes, and thus the appearance of sunspots at a certain latitude should increase the difference of rotation rate between the latitude and the equator. Therefore, the differential of rotation rate in the chromosphere is strengthened by strong magnetic fields. The rotation rate of sunspots is larger than that of photosphere plasma, and thus the appearance of sunspots at a certain latitude should decrease the difference of rotation rate between the equator and the latitude. Therefore, the differential of rotation rate in the photosphere is repressed by strong magnetic fields.

Like an “intruder,” active regions of sunspots form an invasion zone into the quiet chromosphere, namely the so-

called “butterfly diagram,” and the quiet chromosphere superimposed with the butterfly pattern is the observed chromosphere (Li & Feng 2020), as Figure 1 displays here. Similarly, active regions of sunspots, which take along the general rotation characteristics of the tachocline beneath the leptocone, invade the background flow field of the leptocone, forming a low-speed band with the “butterfly diagram” migration, which is the observed zonal flow at the leptocone. At the same time, a high-speed band with the “butterfly diagram” migration (the so-called torsional oscillations) appears in the photosphere (Howard & LaBonte 1980). Therefore in the photosphere, the rotation rate of sunspots is larger than that of the photosphere plasma, and the differential of rotation rate is depressed by the rotation of sunspots. All in all, rotation activities in the solar atmosphere are highly related to the magnetic activities anchored in the solar interior, and SMEs are inferred to originate from the leptocone, while sunspots should come from deeper layers of the interior, probably from the tachocline.

Among the used data of 104 rotations, 7 rotations are missed (Carrington rotations 2041, 2042, and 2091 to 2095), accounting for 6.7% of the total. When the missing data are filled with adjacent Carrington rotations, the obtained result is almost the same as that when missing rotations are left out of

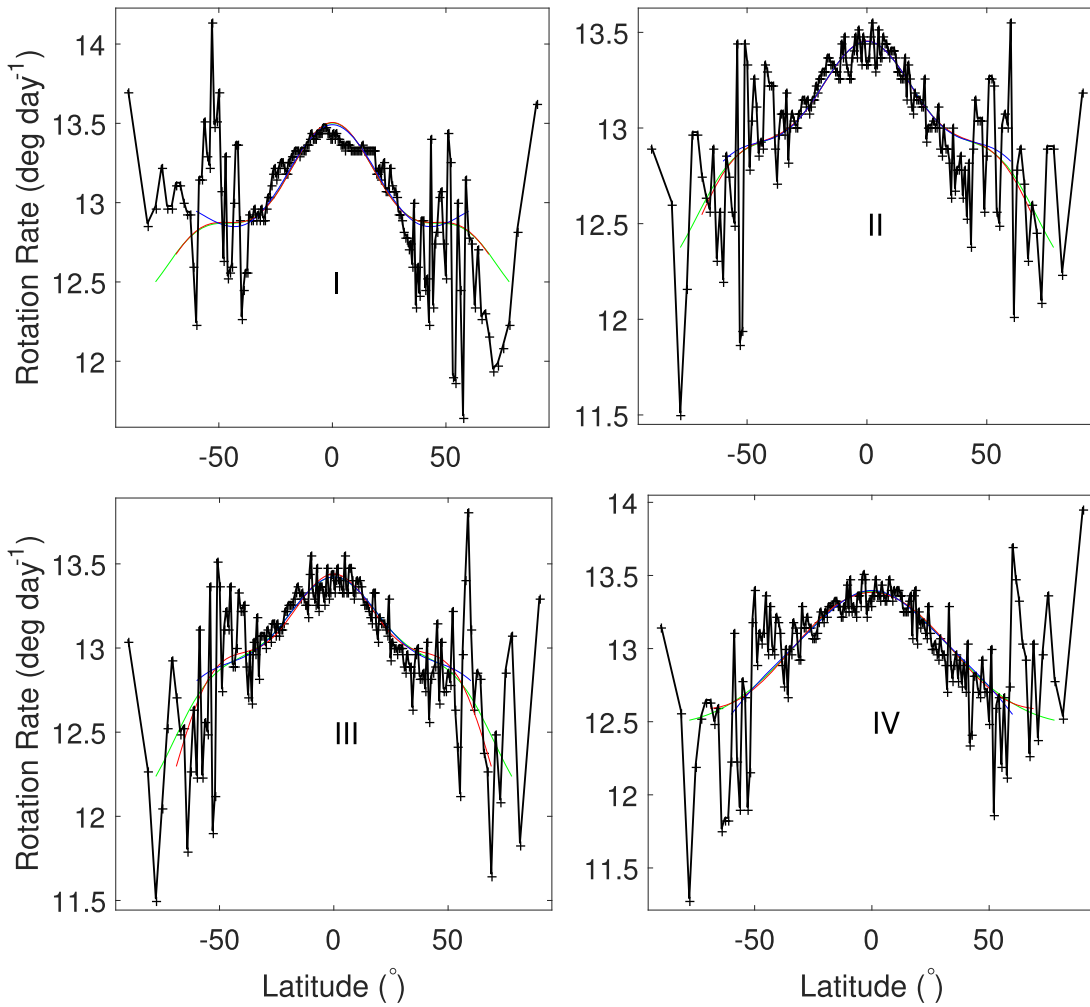


Figure 7. Panel (I): rotation rate (crosses in the black line) at each measurement latitude. The blue, red, and green lines are the fitting lines of those rotation rates whose latitudes are not greater than 60° , 70° , and 80° , respectively. Panel (II): the same as panel (I), but those I_{He} that are not less than -50 are considered. Panel (III): the same as panel (I), but those I_{He} that are not less than -30 are considered. Panel (IV): the same as panel (I), but those I_{He} that are not less than -10 are considered.

the analysis. Therefore, such a small data loss does not have a significant impact on the obtained conclusion.

Synoptic maps of He I intensity are affected by both the projection around the solar poles and the limb darkening, so rotation rates are of lower reliability at high latitudes. This is inferred to be one of the reasons for a large scatter of the chromosphere rotation rates at high latitudes. Zhang et al. (1997) also found a great fluctuation in the rotation rates at high latitudes of over 55° . At high latitudes, the magnetic fields are largely unipolar (Stenflo 1989), and their dependence on time is not explicit (Zhang et al. 1997), that is, it is relatively difficult to distinguish the appearance and disappearance of a single magnetic field in the time series of magnetic fields, so the determination of the rotation rate of magnetic fields is of greatly uncertainty. This is the main reason why the autocorrelation profile of a time series of magnetic fields is wider at high latitudes than that at low latitudes, whose peak overlays a slowly decaying background (Stenflo 1989), and a reason why a large scatter of the chromosphere rotation rates appears here at high latitudes. In this study, latitudes higher than 80° are not considered, and three latitude bands (0° – 60° , 0° – 70° , and 0° – 80°) are separately considered, in order to somewhat present the influence of these factors on the obtained results. In these three cases, rotation rate for the quiet

chromosphere is found to present a decreasing trend from the equator to high latitudes as well, but this finding does not have high credibility and needs to be demonstrated by the precise observations of solar polar regions in the future.

We thank the anonymous referee for careful reading of the manuscript and constructive comments that improved the original version of the manuscript. The full-disk synoptic maps of He I intensity can be publicly downloaded from the NSO’s website. The authors would like to express their deep thanks to the staff of the website. This work is supported by the National Natural Science Foundation of China (11973085, 11903077, 11803086, 11703085, and 11633008), the Yunnan Ten-Thousand Talents Plan (the Yunling-Scholar Project), the national project for large scale scientific facilities (2019YFA0405001), the CAS “Light of West China” Program, and the Collaborating Research Program of CAS Key Laboratory of Solar Activity (KLSA201912, KLSA202012), and the Chinese Academy of Sciences.

ORCID iDs

K. J. Li  <https://orcid.org/0000-0003-3944-9916>

References

- Babcock, H. W. 1961, *ApJ*, 133, 572
- Beck, J. G. 2000, *SoPh*, 191, 47
- Bertello, L., Pevtsov, A. A., & Ulrich, R. K. 2020, *ApJ*, 897, 181
- Bhatt, H., Trivedi, R., Sharma, S. K., & Vats, H. O. 2017, *SoPh*, 292, 55
- Brajsa, R., Pohjolainen, S., Ruzdjak, V., et al. 1996, *SoPh*, 163, 79
- Brajsa, R., Ruzdjak, D., & Wohl, H. 2006, *SoPh*, 237, 365
- Chandra, S., Vats, H. O., & Iyer, K. N. 2010, *MNRAS*, 407, 1108
- De Pontieu, B., De Moortel, I., Martinez-Sykora, J., & McIntosh, S. W. 2017, *ApJL*, 845, L18
- Deng, L. H., Zhang, X. J., Deng, H., Mei, Y., & Wang, F. 2020, *MNRAS*, 491, 848
- Fang, C., Ding, M. D., & Chen, P. F. 2008, *Physics of Solar Active Regions* (Nanjing: Nanjing Univ. Press)
- Fleck, B., Deubner, F. L., Maier, D., & Schmidt, W. 1994, in *Proc. IAU Symp. 154, Infrared Solar Physics*, ed. D. M. Rabin, J. T. Jefferies, & C. Lindsey (Dordrecht: Kluwer), 65
- Golub, L., Harvey, K. L., Herant, M., & Webb, D. F. 1989, *SoPh*, 124, 211
- Harvey, J. W., & Sheeley, N. R., Jr. 1977, *SoPh*, 54, 343
- Harvey, K. L. 1994, in *Proc. IAU Symp. 154, Infrared Solar Physics*, ed. D. M. Rabin, J. T. Jefferies, & C. Lindsey (Dordrecht: Kluwer), 71
- Harvey, K. L., & Livingston, W. C. 1994, in *Proc. IAU Symp. 154, Infrared Solar Physics*, ed. D. M. Rabin, J. T. Jefferies, & C. Lindsey (Dordrecht: Kluwer), 59
- Howard, R. 1984, *ARA&A*, 22, 131
- Howard, R. F. 1996, *ARA&A*, 34, 75
- Howard, R. F., Harvey, J. W., & Forgach, S. 1990, *SoPh*, 130, 295
- Howard, R. F., & LaBonte, B. J. 1980, *ApJL*, 239, L33
- Howe, R. 2009, *LRSP*, 6, 1
- Imada, S., & Fujiyama, M. 2019, *ApJL*, 864, L5
- Javaraiah, J. 2003, *SoPh*, 212, 23
- Jin, C. L., & Wang, J. X. 2012, *ApJ*, 745, 39, 2012
- Jin, C. L., Wang, J. X., Song, Q., & Zhao, H. 2011, *ApJ*, 731, 37
- Komm, R., Howe, R., & Hill, F. 2018, *SoPh*, 293, 145
- Komm, R., Howe, R., Hill, F., & Hernandez, I. G. 2009, *SoPh*, 254, 1
- Lamb, D. A. 2017, *ApJ*, 836, 10
- Lefebvre, S., Nghiem, P. A. P., & Turck-Chieze, S. 2009, *ApJ*, 690, 1272
- Li, K. J., & Feng, W. 2019, *MNRAS*, 489, 3427
- Li, K. J., & Feng, W. 2020, *MNRAS*, 497, 969
- Li, K. J., Xie, J. L., & Shi, X. J. 2013, *ApJS*, 206, 15
- Li, K. J., Xu, J. C., & Feng, W. 2018, *ApJS*, 237, 7
- Li, K. J., Xu, J. C., Yin, Z. Q., & Feng, W. 2019, *ApJ*, 875, 90
- Livingston, W. C., Harvey, J., Pierce, A. K., et al. 1976, *ApOpt*, 15, 33
- Parker, E. N. 1991, *ApJ*, 372, 719
- Shi, X. J., & Xie, J. L. 2013, *ApJL*, 773, 6
- Snodgrass, H. B., Howard, R., & Webster, L. 1984, *SoPh*, 90, 199
- Stenflo, J. O. 1989, *A&A*, 210, 403
- Sudar, D., Saar, S. H., Skokic, I., Poljancic Beljan, I., & Brajsa, R. 2016, *A&A*, 587, A29
- Vats, H. O., & Chandra, S. 2011, *MNRAS*, 413, L29
- Xiang, N. B., Ning, Z. J., & Li, F. Y. 2020, *ApJ*, 896, 13
- Xiang, N. B., Qu, Z. N., & Zhai, Q. 2014, *AJ*, 148, 12
- Xu, J. C., & Gao, P. X. 2016, *ApJ*, 833, 144
- Zhang, L. D., Zirin, H., & Marquette, W. H. 1997, *SoPh*, 175, 59